Eidgenössische Technische Hochschule Zürich
Swiss Federal Institute of Technology Zurich

SED
Schweizerischer Erdbebendienst
Swiss Seismological Service

Report on site characterization

Stiegenhof - Oberembrach (STIEG)

Poggi Valerio, Clotaire Michel, Donat Fäh

Last modified - 04 / 04 / 2013

1. Introduction

In the framework of the NAGRA seismic network project, an array measurement of the ambient vibration wave-field was performed on 24/01/2013 at the location of the SED borehole station STIEG (Stiegenhof, Oberembrach). The scope of the survey is the seismic characterization of the area surrounding the installation, which consists in a short-period borehole sensor at about 100m depth, with a collocated strong motion sensor at the surface. Ambient vibration analysis has been used to infer the characteristics of the underground structure of the site, with special regard to the shear-wave velocity at the site. Such profile was later compared with the results from active seismic measurements and used to assess the local seismic response of the station.

For the analysis, different spectral analysis techniques were implemented, consisting in both single and array methods which are listed below:

- Time-frequency wavelet analysis
- Power-spectral density estimation
- Conventional horizontal to vertical spectral ratios
- Directional horizontal to vertical spectral ratios
- Wavelet polarization analysis
- Three-component high-resolution f-k analysis.

In the following, the main results of these investigations are summarized and a final interpretation of the velocity profile is given. From this interpretation, engineering parameters are finally derived, e.g. the Qwl-Vs average velocity, VsZ (including Vs30) and the seismic amplification from the analytical SH-transfer function of the one-dimensional soil column.

2. Survey description

To characterize the seismic response of the site, an array measurement of ambient vibration has been performed (**Figure 1**). The array consisted in two measuring configurations (A and B) of 14 sensors each and different diameters of 100m and 200m respectively. The two configurations were planned to partially overlap, by sharing 9 common sensors, with the aim of providing a continuous resolution of the frequency range between the two geometries. Configuration A recorded for a total of 1h40m, while configuration B for 2h15m. The differences in the recording length are due to the different resolution characteristics of the two geometries. As a general rule, larger arrays require longer recording time to produce a reasonable statistics of the ambient vibration processing results. For the larger configuration, a penetration depth of 80-100m was expected.

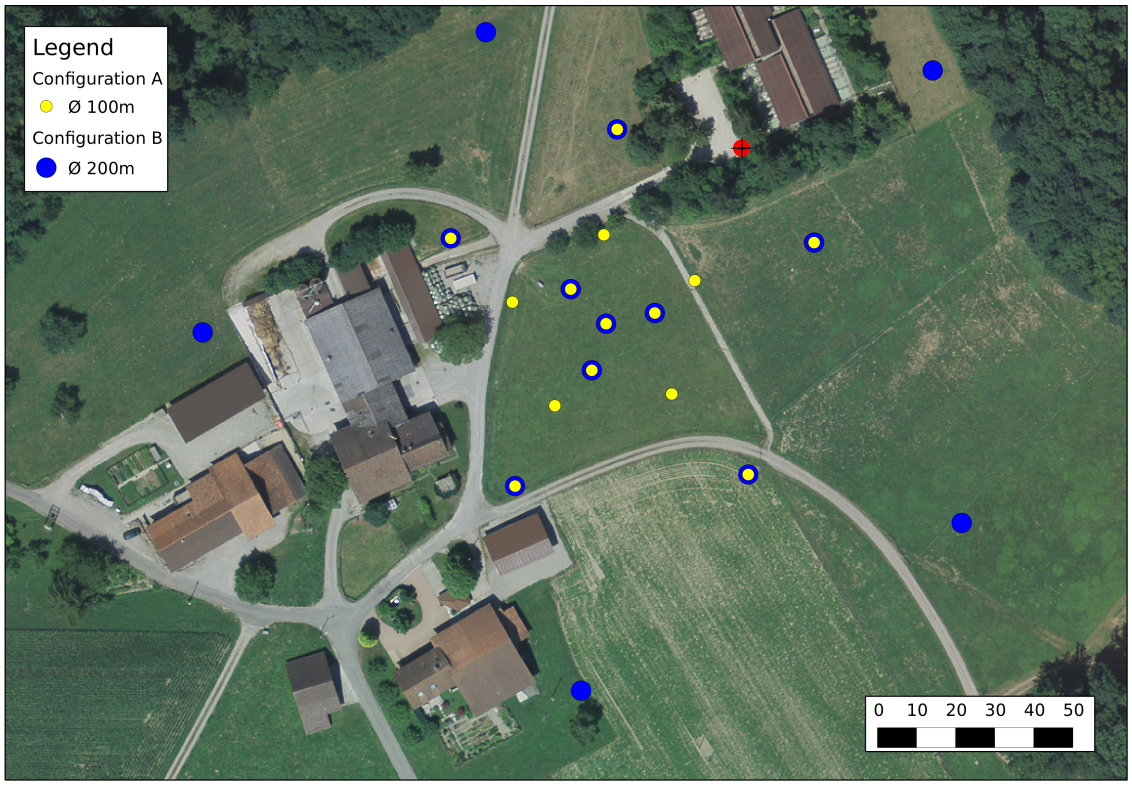

Figure 1 - *Geometry of the ambient vibration arrays in Stiegenhof (SED station STIEG). Two concentric configurations of increasing diameter were used. The borehole station location is shown in red.*

3. Soil type, topography and geology

The array has been set in open field conditions, in a rural area (**Figure 1**). Influence of buildings and anthropogenic disturbances is virtually negligible. Sensors have been mostly deployed on free soil conditions. Good coupling with the ground was assured by means of digging small holes at the sensor's places, and by using a special support (Trihedron) that facilitates the leveled accommodation of the device even in difficult soil conditions. The measurement area is located on a gentle slope toward southeast. However, no topographic correction has been accounted before processing.

From the geological points of view (**Figure 2**), the target area is located within the Molasse basin, surrounded by few moranic deposits, clearly identifiable from the surface topography. The bedrock probably consists of siltstone and marl, with intercalations of some under-consolidated sandstone and occasionally conglomerates. The site can be geotechnically classified as of rock ground-type A. The drilling log report of the borehole can be found in the appendix.

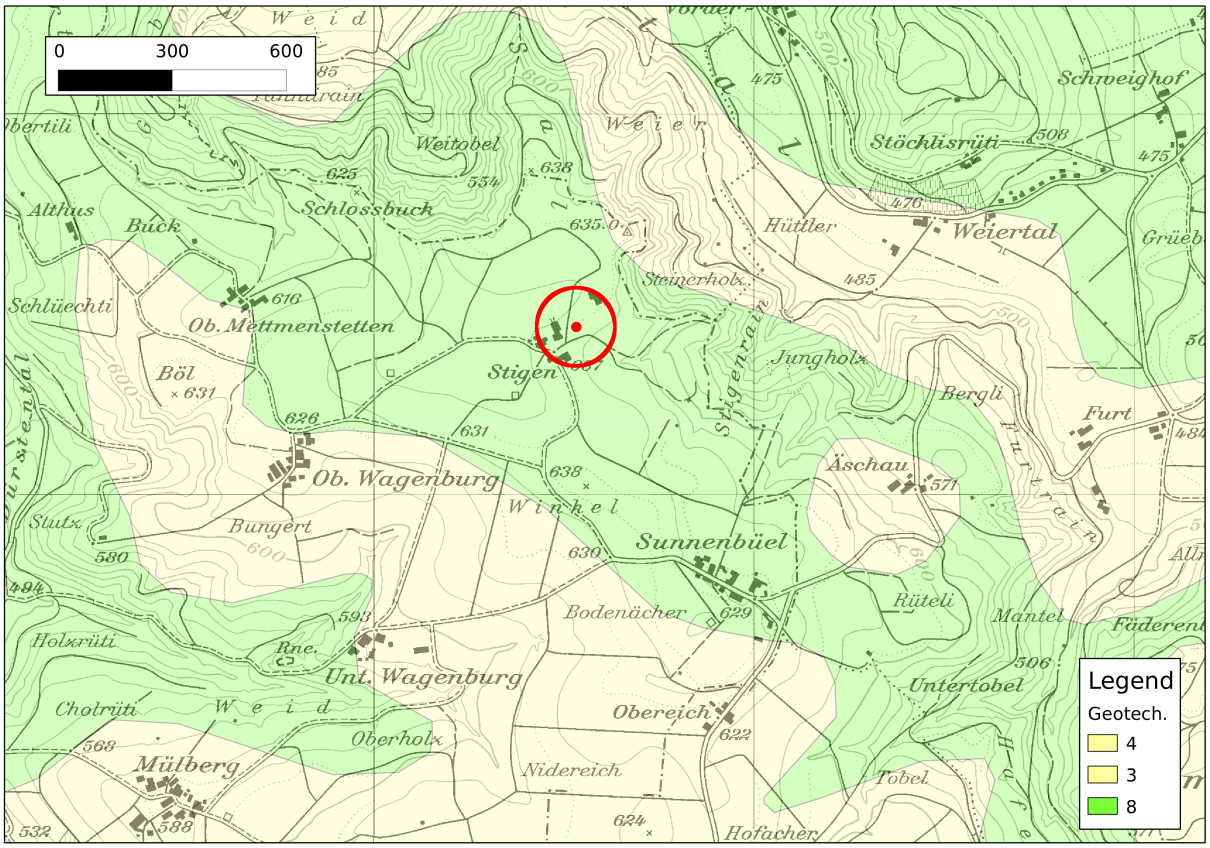

Figure 2 - *Geological map of the area of the array measurement in Stiegenhof (Legend: 3, morain; 4, fluvio-lacustrine deposits; 8, marl and conglomerates; from SWISSTOPO).*

4. Acquisition equipment

Each acquisition point within the array consisted of a three components seismometer (Lennarz 3C with 5s eigenperiod, **Figure 3**) and a 24 bit data logger (Quanterra Q330). Synchronization between stations was assured by standard GPS, while a more accurate differential GPS (Laica Viva system) was used to precisely locate the sensor's coordinates with a tolerance of less than 5cm.

5. Weather conditions

The weather conditions were stable during the whole measurement, with no precipitations and an average (over the whole day) temperature of -2 degrees. It has to be notice the presence of few centimeters of frozen snow on the ground. The cold temperature and the snow cover may be considered an advantage in this case, due to the increase in the stiffness of the soil's top cover, which consequently improves the coupling between sensors and ground.

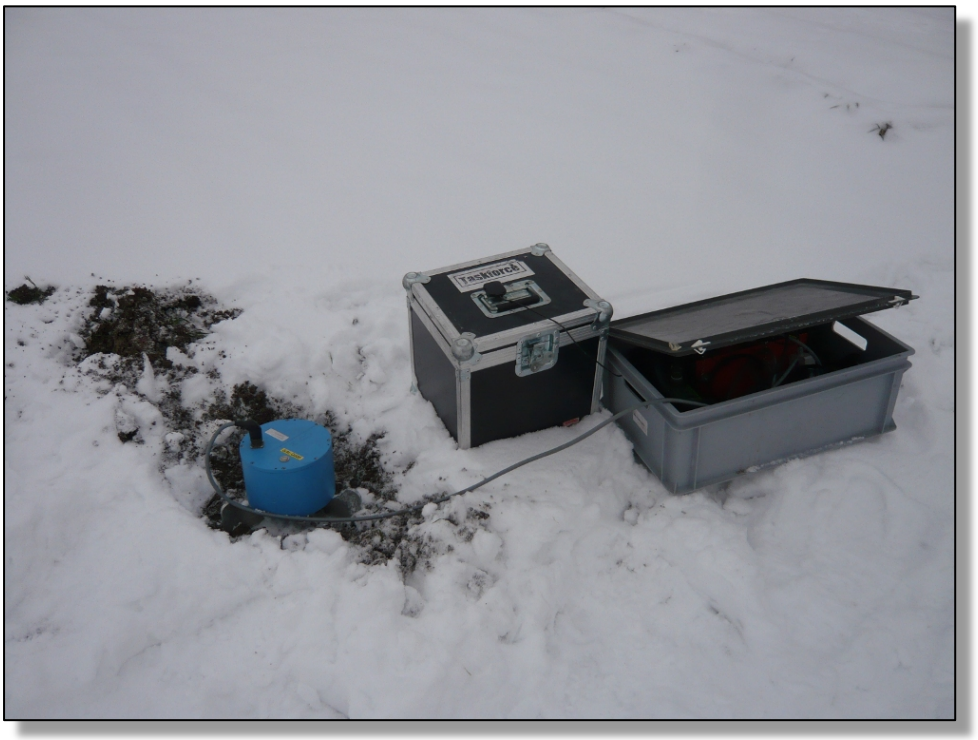

Figure 3 - *Single acquisition point of the array, consisting in a Q330 datalogger (gray box on the right) and a Lennartz 5s velocity seismometer (blue, on the left). The coupling of the sensor is assured by removing the uppermost part of the frozen soil and by means of a special support (Trihedron).*

6. Pre-processing and preliminary data-quality control

The three-component recording has been filtered prior to analysis using a high-pass 6th order causal Butterworth filter with corner at 0.2Hz. Although it is not a strict requirement for spectral analysis techniques, such filtering was applied in order to facilitate the preliminary visual inspection of the noise traces (**Figure 4**).

To assess the quality of the ambient vibration recordings, spectral analysis has then to be performed. Because of the stochastic nature of the ambient vibration wave-field, a statistical approach has to be used, such as the estimation of the power spectral density (*PSD*). This approach is useful to evaluate the average energy level of the recordings in the analyzed frequency range, and to access the presence of spurious spectral peaks, which might be related to human activity (machinery, pumps). By inspecting the PSD of the three-component recordings at the central station (e.g. **Figure 5**), no relevant spurious peak is visible in the range between 0.5 and 40Hz. The average noise level is quite low and within the minimum and maximum bounds of the USGS noise model.

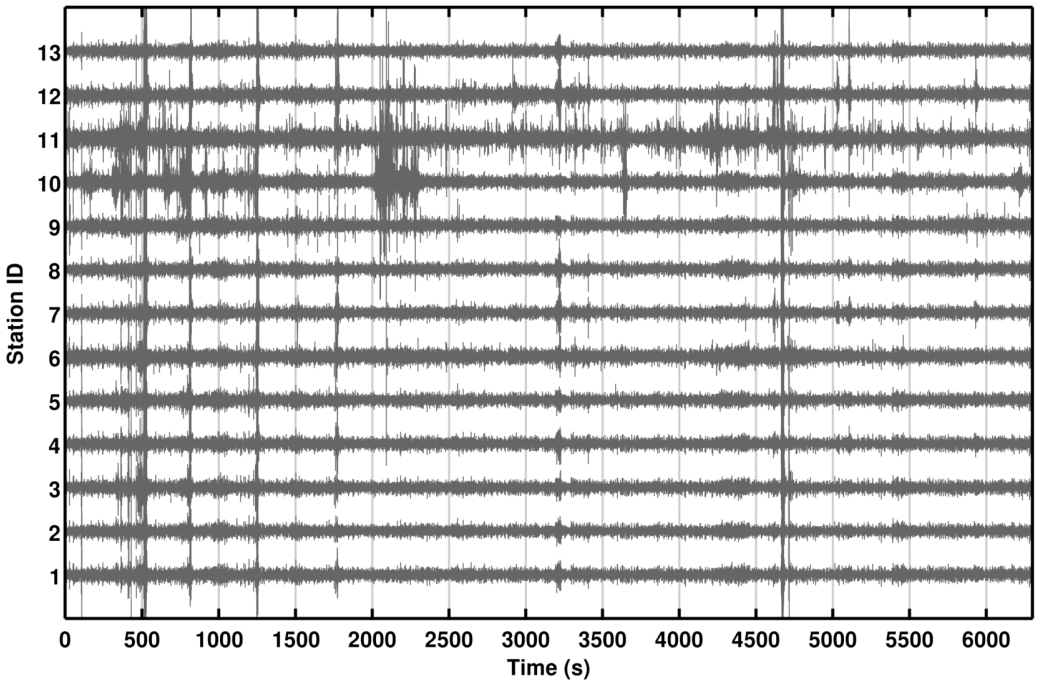

Figure 4 - *Inspection of the useful part of the ambient vibration recording of the array STIEG (configuration A). Several impulsive high-frequency transients of anthropogenic origin (usually > 40Hz) are visible, but the overall quality of the recording is good.*

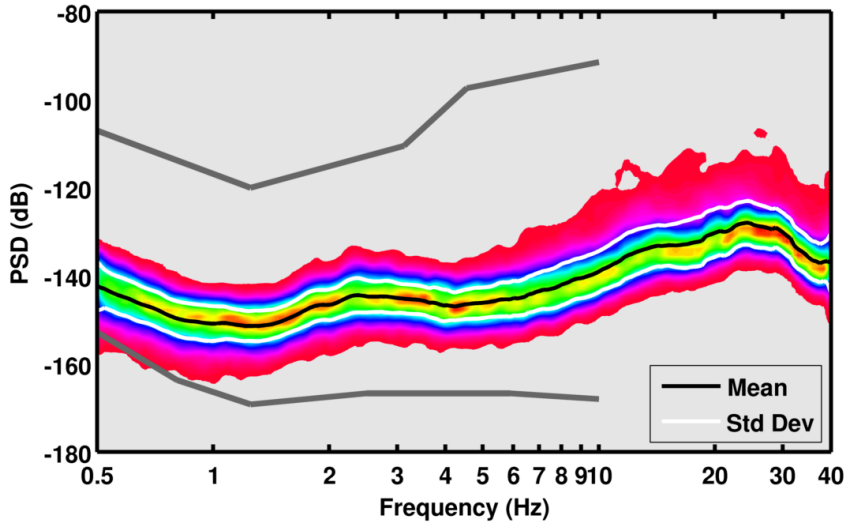

Figure 5 - *Power spectral density (PSD) computed for 1h recording at the central station of the array (here the vertical component is presented). In gray are the minimum and the maximum bounds of the USGS noise model, for comparison.*

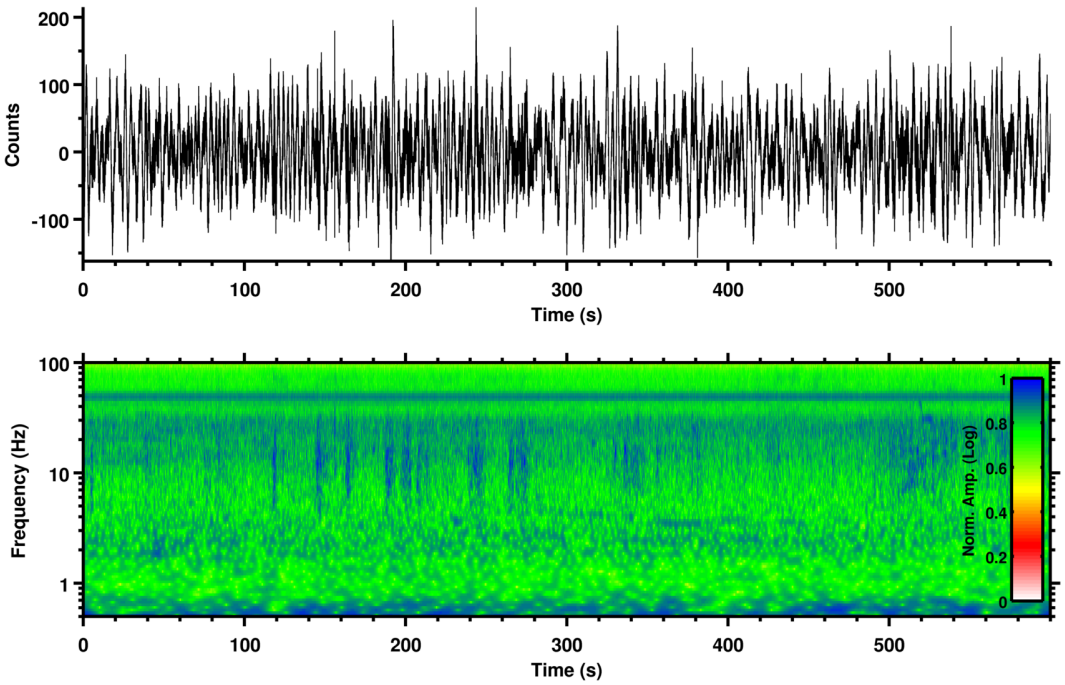

Figure 6 - *Example of spectrogram from 600s of recording of the array central station (A1, vertical component). For the analysis, the cosine wavelet is used (wavelet parameter = 12).*

Complementary to statistical methods, then, a spectral decomposition approach is more suitable to assess the stationarity of the ambient vibration wave-field over time. The wavelet time-frequency analysis was then performed over the whole recording time. From such analysis (**Figure 6**) an overall stability of the ambient-vibration wave-field over time is evident. The only clear disturbance is the 50Hz signal from the electric power line, which is nevertheless not an issue because of the frequency outside the range of interest, and its narrow and well-defined localization in the spectrum.

7. Conventional H/V spectral ratios

The horizontal-to-vertical (H/V) Fourier spectral ratio is a technique widely used in seismic site characterization because of its ability to provide an estimate of the SH wave fundamental frequency of resonance (f_0) of the site. Other than that, H/V ratios are useful to provide information on the Rayleigh wave ellipticity function, which is used in the inversion procedure to constrain the major velocity contrasts at depth. In this study, we use the technique also to map the variability of the subsoil structure along the investigated area; this is necessary to verify the fulfillment of the 1D structure assumption, which is necessary for the f-k method applied later.

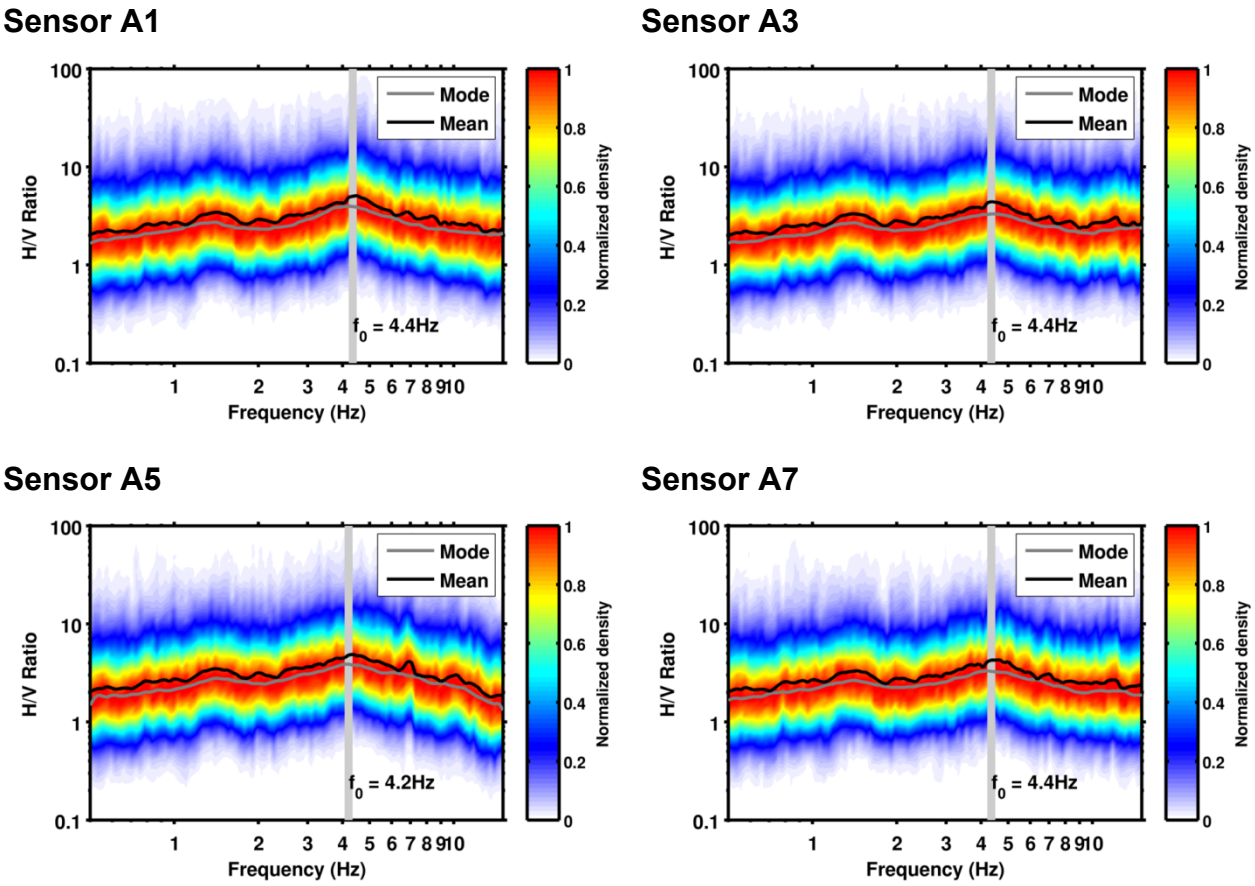

Figure 7 - *Example of H/V spectral ratios at four stations of the array configuration A. The picked fundamental frequency is indicated with a light gray line.*

H/V spectral ratios have been computed for the recordings at each station of the two array configurations (e.g. **Figure 7**). The behavior of the noise wave-field at the different stations location is comparable (**Figure 8**). For the first ring, no strong variation of the fundamental frequency is observed across the area, with an average value of about 4.4Hz. Also the shape of the spectral ratios is very similar, with the only exception of the station A13 (from the external border) that shows a slight decrease in the spectral amplitude below f_0. This can be due to a small change of the velocity in the deeper part of the profile toward south-west. The second ring provides similar results, even if the fundamental frequency is less precisely localized at 4.4Hz, and a small amplitude peak is visible at 1.2Hz. The behavior of the site can be considered laterally homogeneous for the f-k analysis.

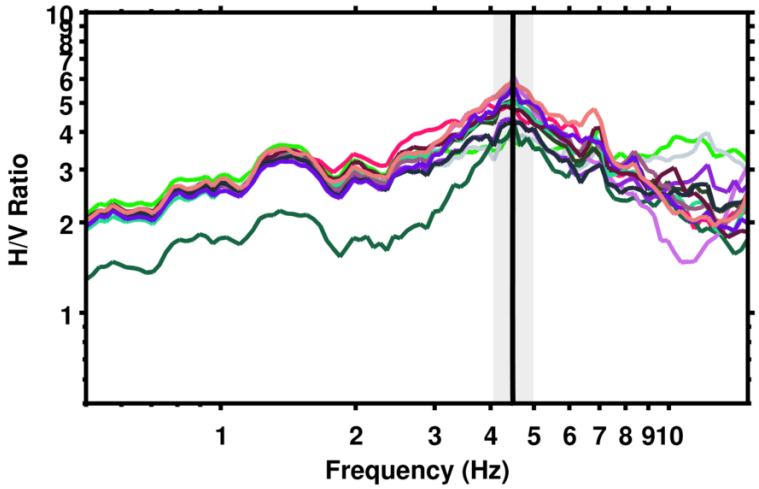

Figure 8 - *Comparison of the H/V spectral ratio curves of all the stations of the array configuration A. Only one station (A13) shows a different behavior at low frequencies, while the fundamental frequency does not change.*

8. Direction H/V spectral ratios

The computation of directional H/V spectral ratios is useful to reveal asymmetries in the ambient vibration wave-field. Such a behavior can be induced by several reasons: 2D/3D structure, topographic effects or a not homogeneous distribution of the noise sources. If a strong directionality is found by the analysis, it is generally recommended to carry out further investigations to properly address the origin of polarization.

By processing the directional H/Vs at all the recording stations of the array (e.g. **Figure 9**) it is possible to observe a very small directionality of the main resonance peak at 4.4Hz. The observed direction is rather stable over the whole array, at about 160°N. Considering that this effect is mostly visible at f_0, we interpret it as an influence of the topographic slope or a small 3D effect. A non-homogenous distribution of the noise sources should be excluded, even if such interpretation has to be validated by the subsequent results of the f-k analysis.

The result of the directional analysis is also confirmed by applying the wavelet polarization analysis techniques as described in Burjanek et al. (2008) to the central station of the array. Also in this case the fundamental frequency shows a moderate directionality (**Figure 10**a), but not a significant polarization (**Figure 10**b).

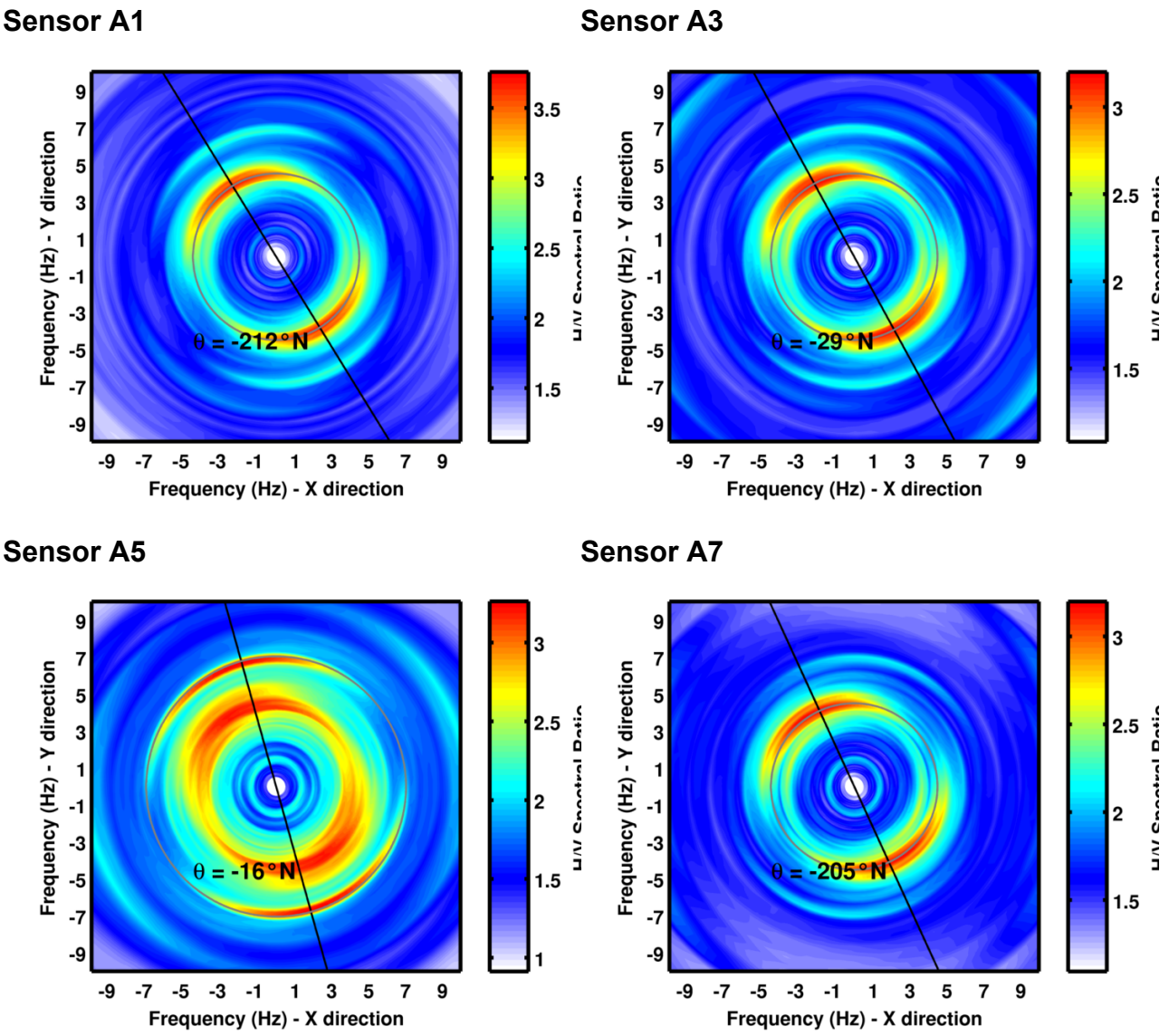

Figure 9 - *Example of directional H/V spectral ratios at four stations of the array configuration A. The fundamental frequency shows some very small directionality effect along NNW-SSE. This might be related to the moderate topography slope.*

a)

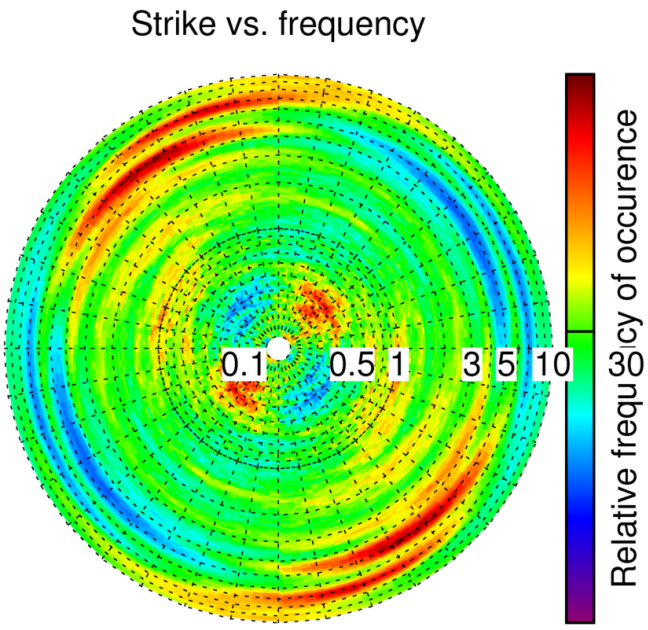

b)

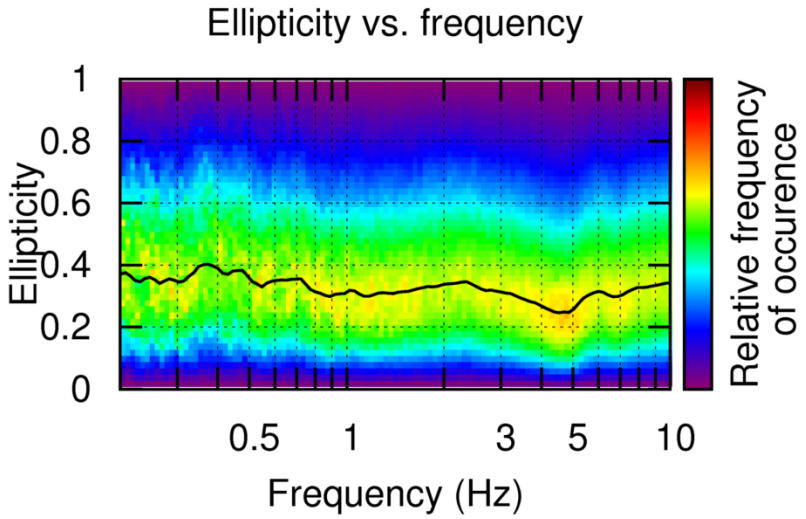

Figure 10 - *Wavelet-based polarization analysis at the central station of the array. By analyzing the polarization over strike (a) and the particle motion ellipticity plot (b), only a moderate directional effect is visible at the resonance frequency.*

9. Three-component f-k analysis

The frequency-wavenumber analysis is a spectral technique based on seismic array recordings that allows retrieving the direction and the dispersion characteristics of the surface wave-field. We apply here this technique to three-component ambient vibration recordings using a modification of the high-resolution method of Capon (1969) as described in Poggi et al. (2010). Using all the three-components of motion gives the possibility to retrieve information about the propagation of the Rayleigh waves (vertical and radial processing direction) as well as of the Love waves (transversal direction).

As in the case of the previous methods, the ambient vibration recordings are treated statistically by subdividing the traces in sub-windows. For each consecutive window a separated f-k analysis is performed, and the results are then averaged over the whole recording, to strength the robustness of the final estimation.

a) 4.4 H (Resonance frequency)

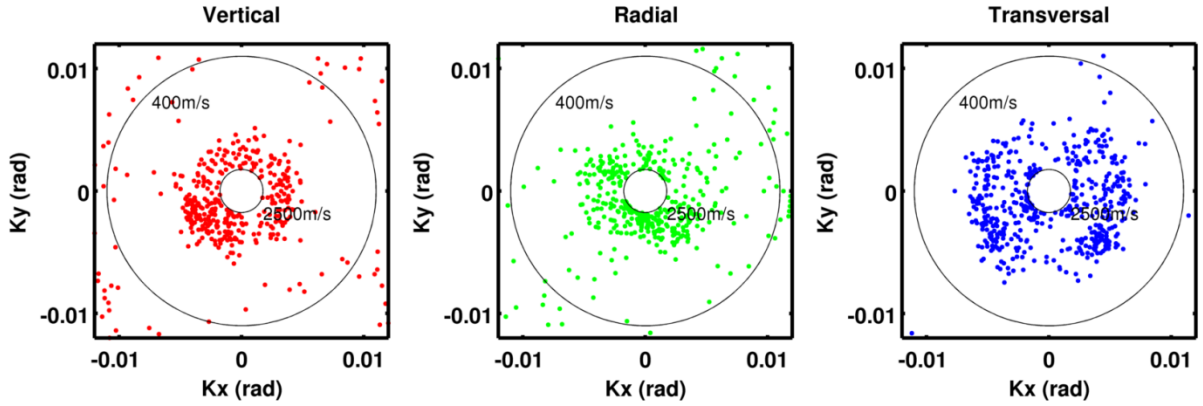

b) 6 Hz

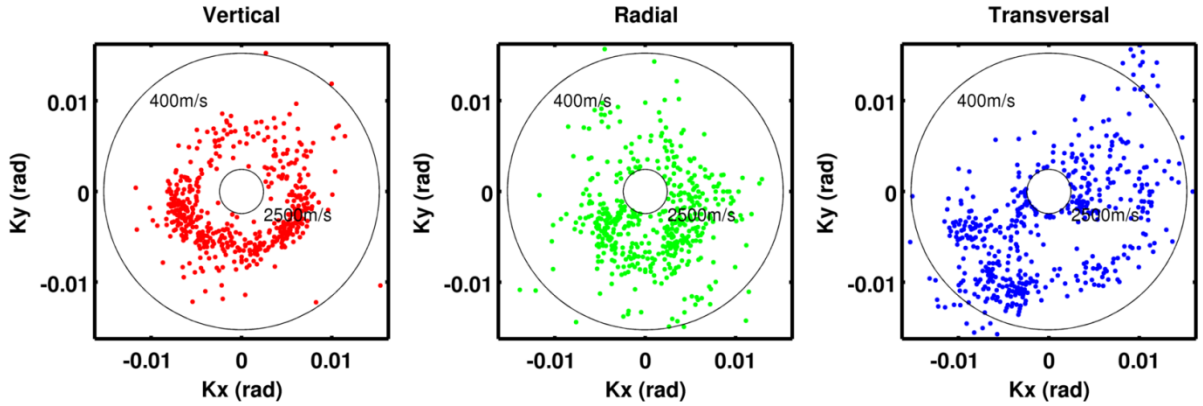

Figure 11 - *Example of distribution of noise sources at 6Hz over the three components of the f-k analysis (here for array configuration B). Distribution is homogeneous for the vertical and radial directions, with only some moderate directionality on the transversal direction at 6Hz.*

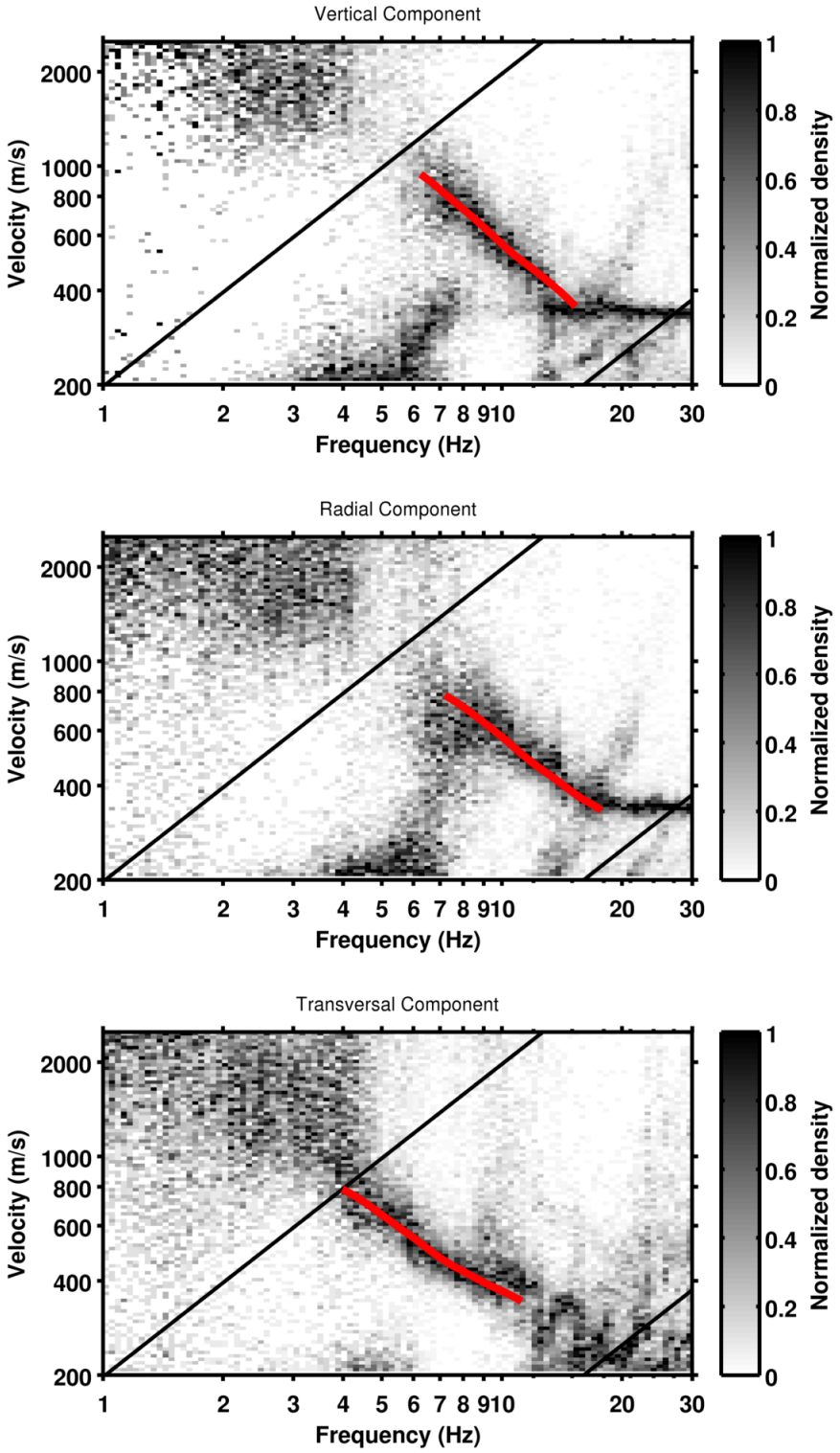

Figure 12 - *Density distribution of all the surface wave signals obtained from the whole recording of array configuration A using f-k analysis. In red is the interpreted dispersion curve (manually selected).*

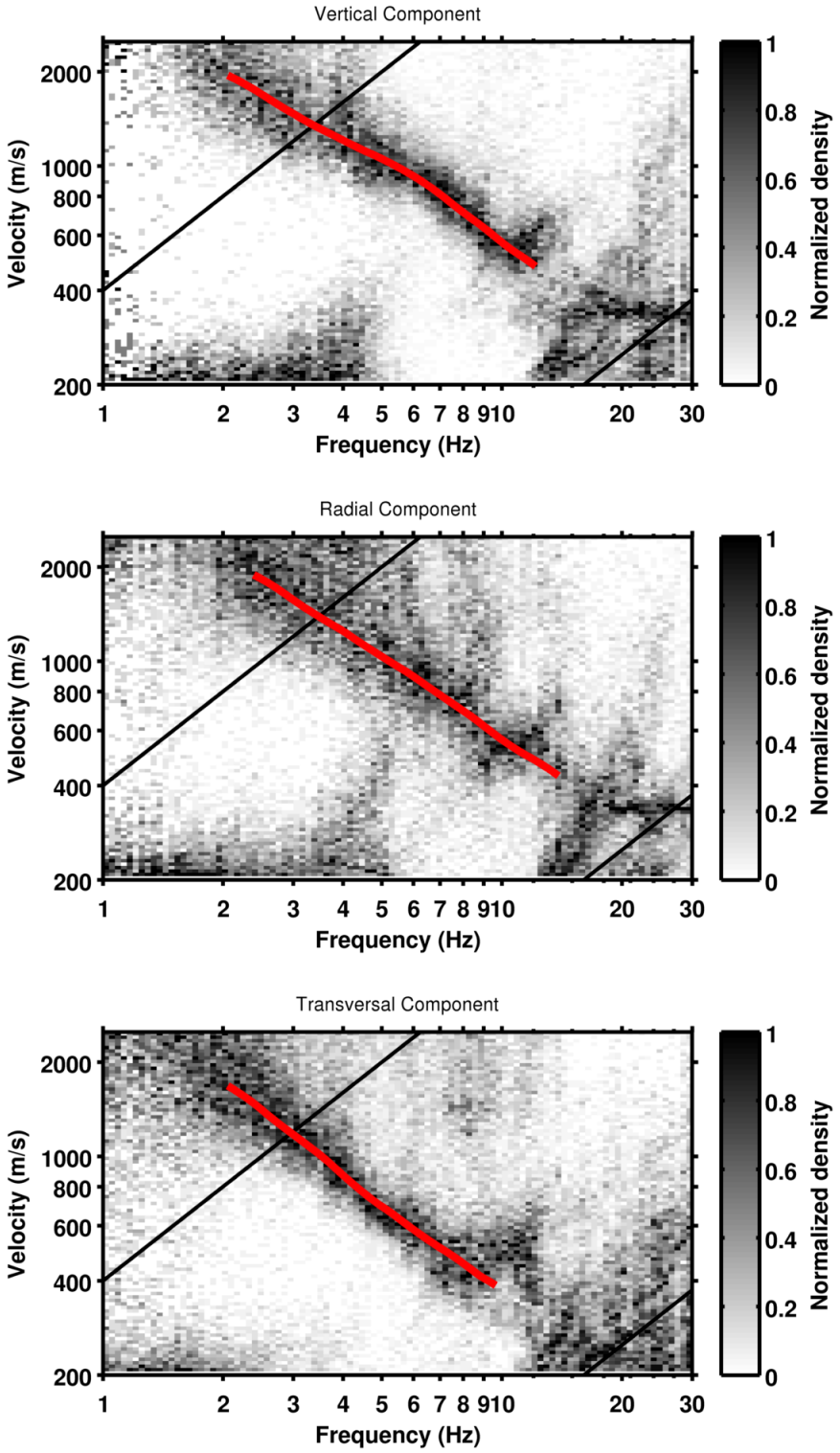

Figure 13 - *Density distribution of all the surface wave signals obtained from the whole recording of array configuration B using f-k analysis. In red is the interpreted dispersion curve (manually selected).*

As first step, from the f-k analysis it was possible to assess the noise source distribution over broad range of analyzed frequencies (e.g. **Figure 11**) for the vertical, the radial and the transversal component. A rather uniform (isotropic) distribution is observed, and particularly at f_0, confirming then the independency of the noise source distribution to the directional behavior observed in the H/V spectral ratio. Subsequently, the surface wave dispersion curves have been extracted by visual inspection and manual picking of the f-k density plots (**Figure 12** and **Figure 13**). It has to be noticed that the two array configurations provided comparable results, but in different frequency bands (which is consequence of the array geometry), which are nevertheless overlapping. The final interpretation of the modal dispersion pattern is presented in **Figure 14** for both the Rayleigh and Love waves.

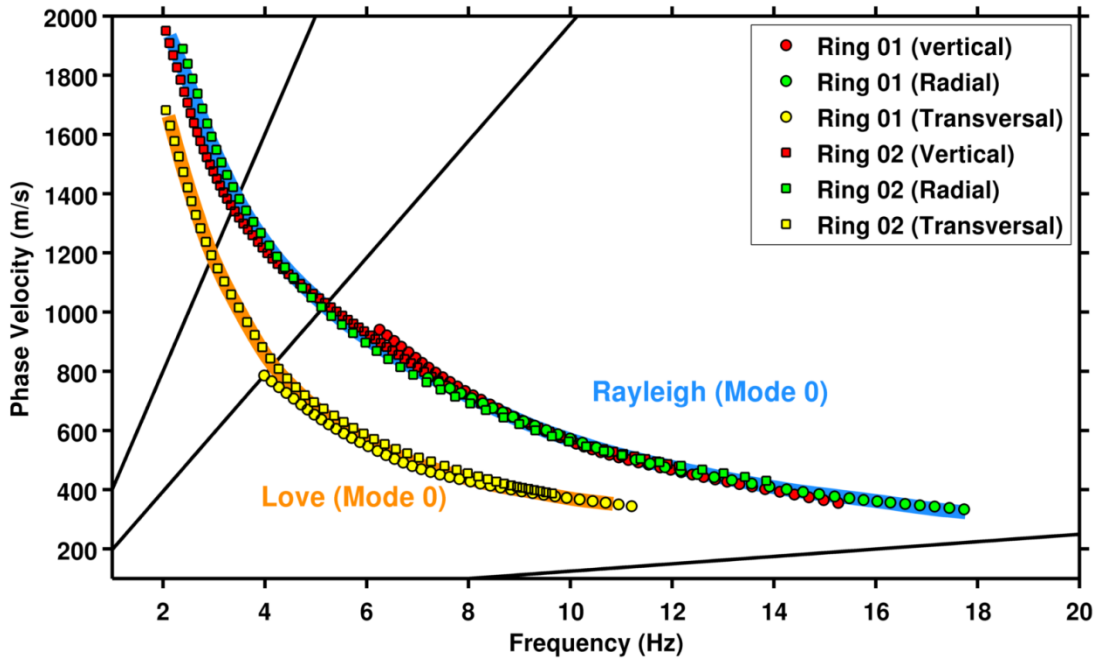

Figure 14 - *Final interpretation of the Rayleigh and Love dispersion modal pattern from the two concentric array configurations.*

10. Inversion of the dispersion curves

The surface wave dispersion curves (Rayleigh and Love) obtained from the three-component f-k analysis of the ambient vibrations were inverted to obtain an estimation of the velocity profile of the site (mainly S-wave velocity as function of depth, and to a lesser extend the P-wave velocity, due to the lower sensitivity). The analysis was performed using the software *Dinver* (www.geopsy.org), which implements a direct search approach (**Figure 15**) based on a conditional version of the neighborhood algorithm (Sambridge 1999).

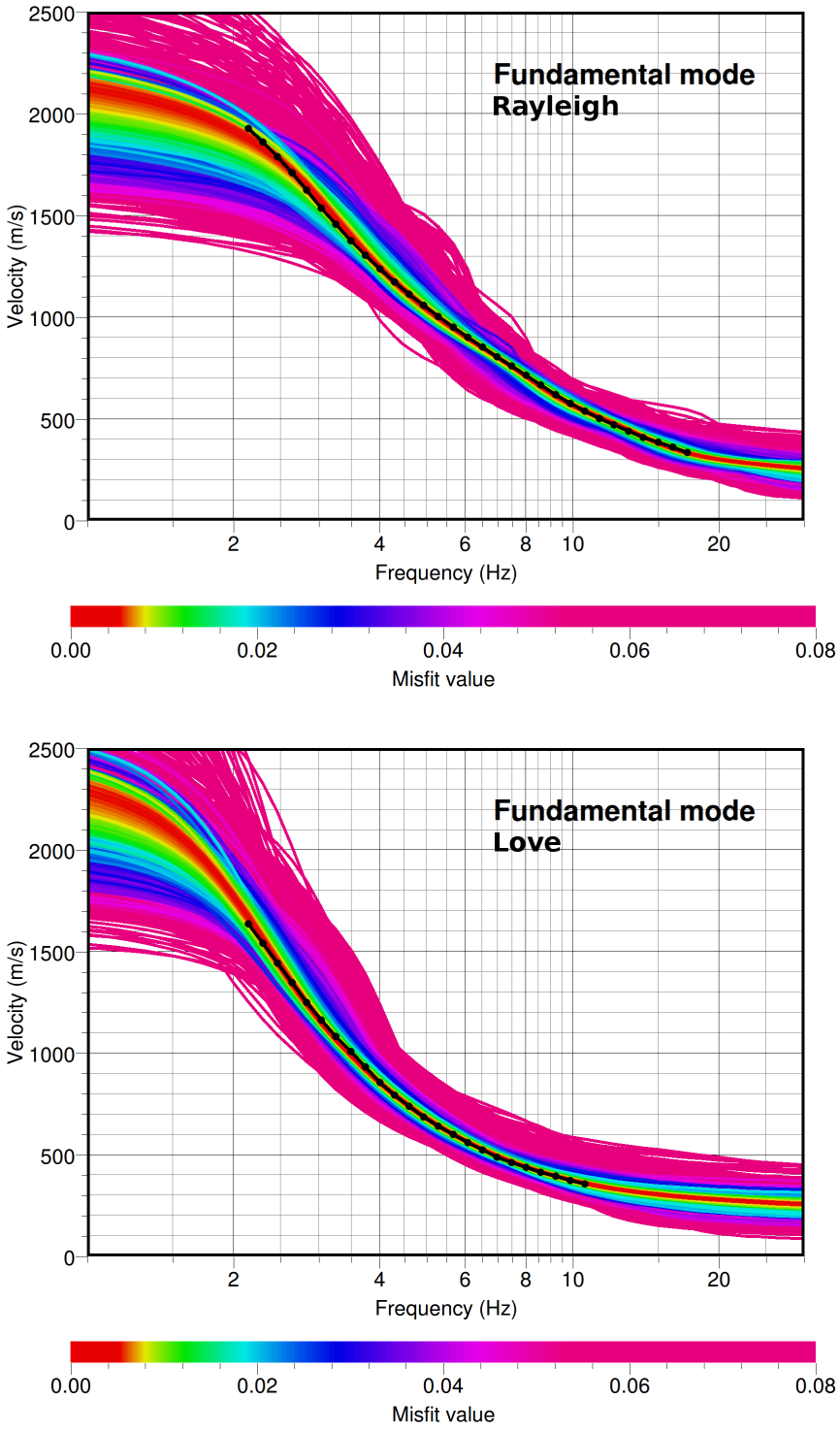

Figure 15 - *Fitting the surface dispersion data within the global optimization procedure. Different colors represent different misfit between the observed (in black) and the modeled dispersion curves.*

Together with the dispersion curves, the fundamental frequency of the Rayleigh-wave ellipticity function obtained from the H/V spectral ratio was used as constraint for the inversion. Using such additional information is advantageous to improve the resolution on the larger velocity interfaces of the model. To parameterize the velocity model, two different approaches were implemented. The first one consisted in setting up an eight-layer model with free interface depths (**Figure 16**). In such a case the free inversion parameters are then the velocities (P and S) and layer thicknesses. In the second case, a fixed-thickness layer approach was used (**Figure 17**). The advantage of the former method stays in the possibility to better resolve sharp velocity interfaces, while the second is less unique and better constraints the seismic velocity. The two approaches have to be nevertheless considered complementary, and they should provide consistent results.

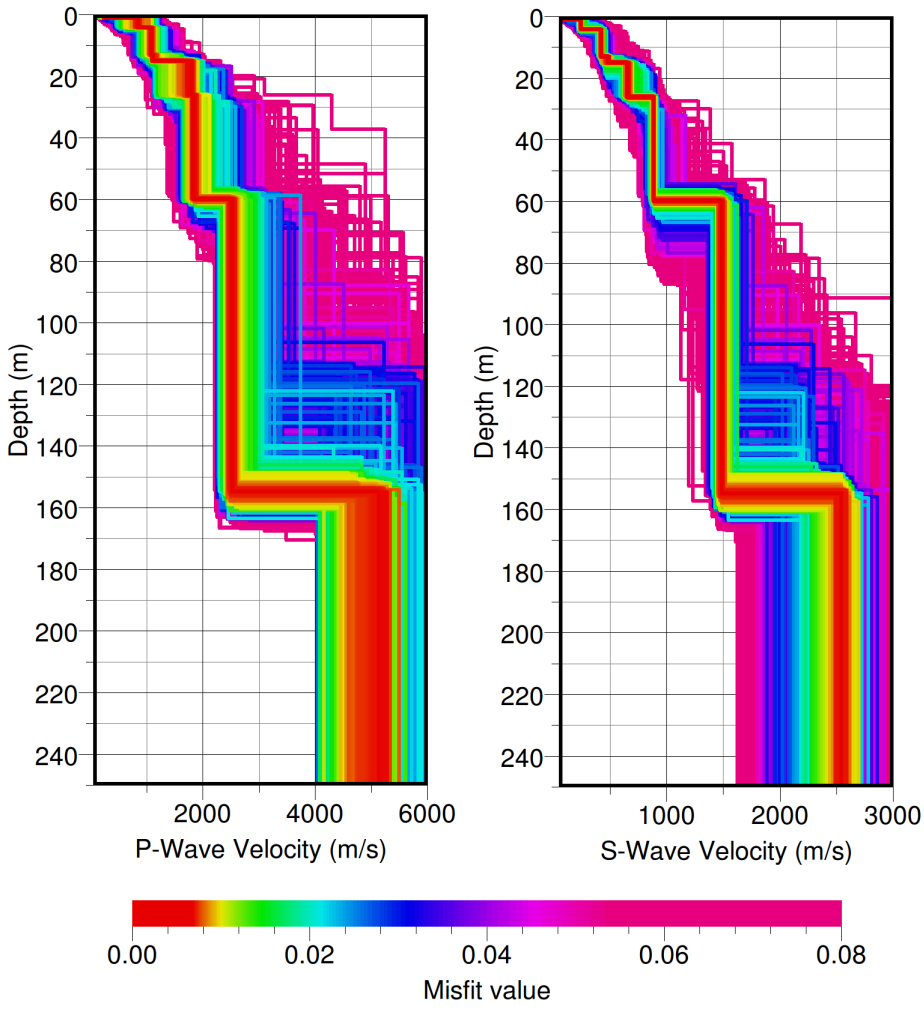

Figure 16 - *Distribution of the free-layer velocity models generated during the inversion process and ordered by decreasing misfit, according to the color scheme of* **Figure 15**.

Eight inversion tests (*runs*) have been performed for each of the two model schemes (**Figure 18**). This in order to minimize the effect related to a possible unfavorable initial randomization of the space parameter. The best fitting models from of each run are then collected and used later on for the computation of the derived soil parameters.

The inverted velocity models (Vs and Vp) are gradient like, with a faster increase in velocity in the first 10~20m, followed by a more smoothed part. This is expected for a rock velocity profile. By considering the minimum available frequency of the surface-wave dispersion curves, and by analyzing the scattering of the inverted models (**Figure 19**), it is realistic to assume the velocity profiles to be reliable down to a depth of about 100~120m. Below this value no direct constrain is available, and the velocity are obtained by pure extrapolation.

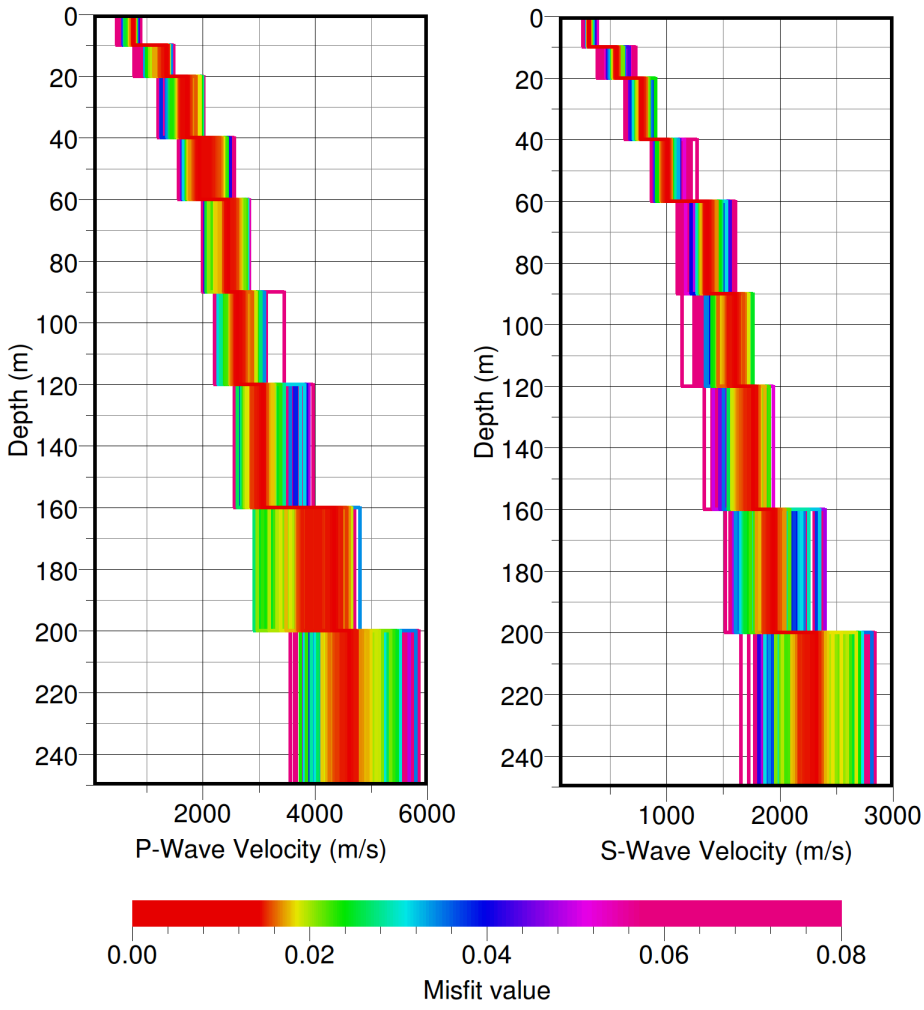

Figure 17 - *Distribution of the fix-layer velocity models generated during the inversion process, and ordered by decreasing misfit according to the color scheme of* **Figure 15**.

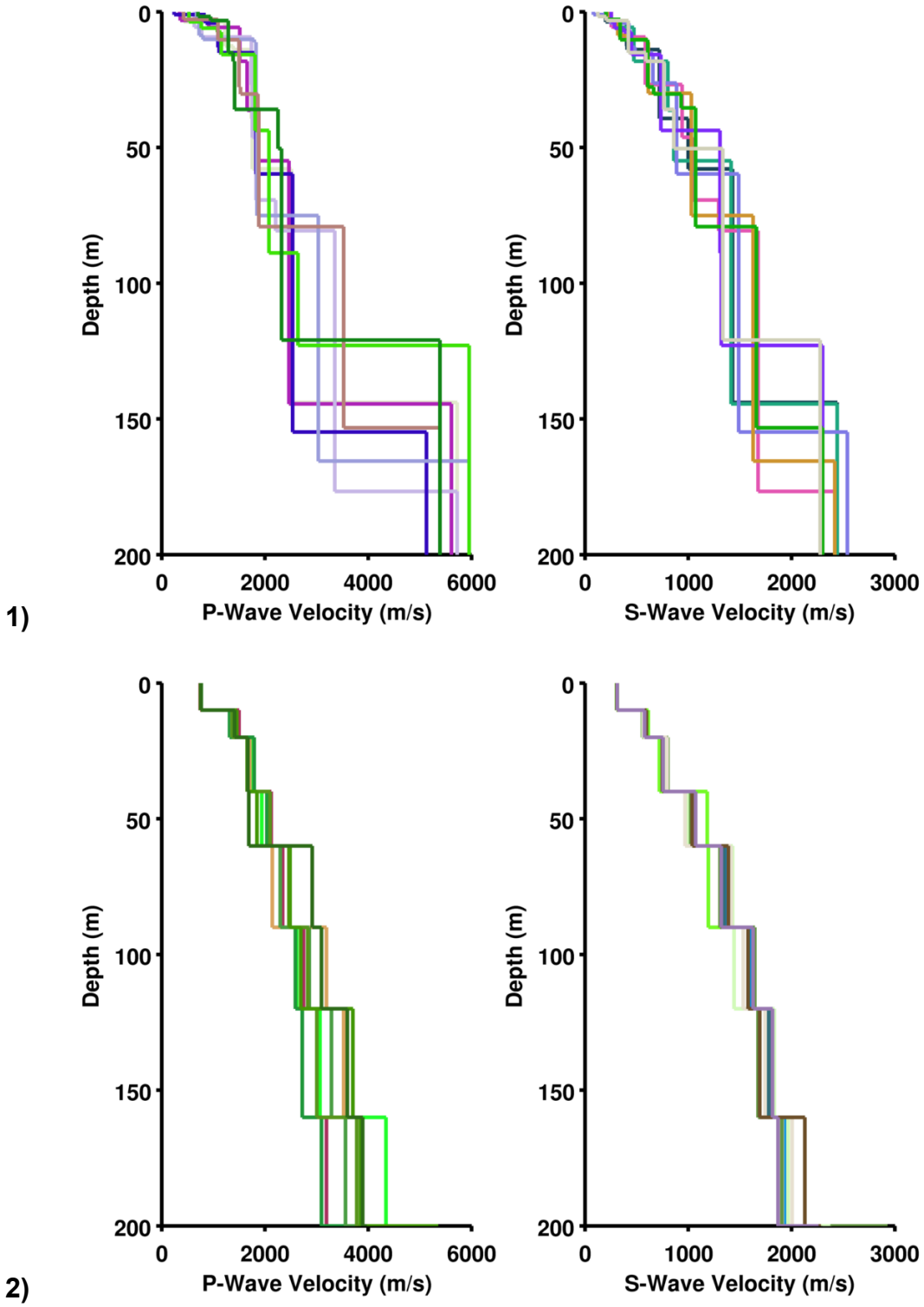

Figure 18 - *Collecting the best fitting models from the eight separated inversion runs using the free-layers (1) and fixed-layers (2) parameterization schemes.*

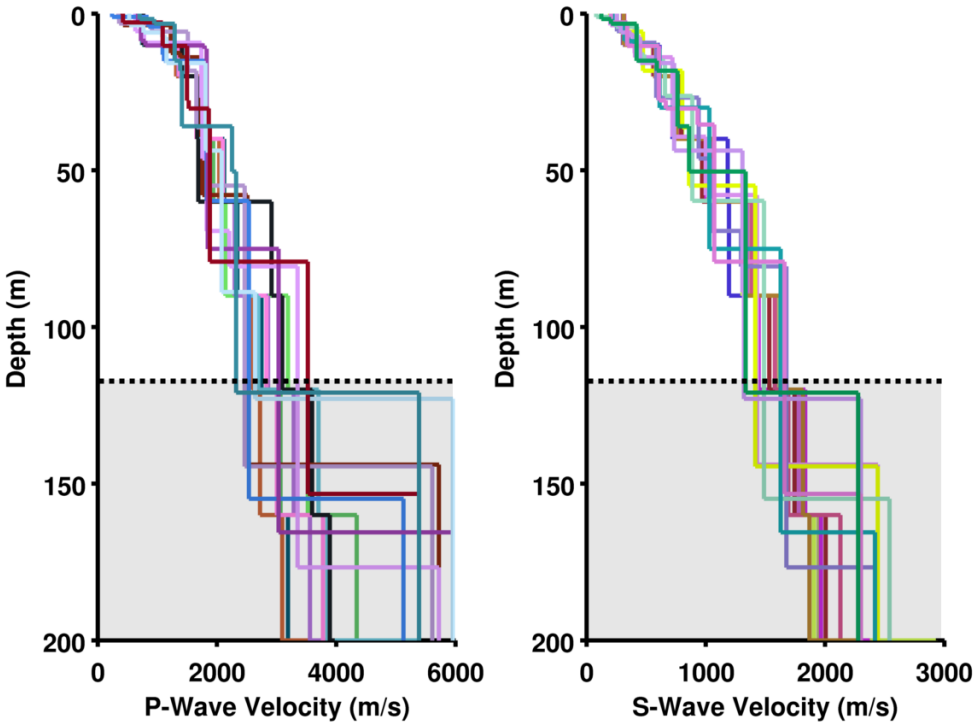

Figure 19 - *Comparison of all the best models from the two parameterization schemes (free and fixed layers). The two approaches are consistent down to a depth of about 100~120m, which can be considered the maximum resolved depth.*

11. Engineering soil parameters

The ensemble of all the best inverted velocity profiles is then used to derive average soil parameters like the VsZ (average travel-time S-wave velocity over the depth Z, including Vs30, Table 1) and the quarter-wavelength (QWL) average velocities (Joyner et al., 1984) for a range of frequencies between 0.8 and 15Hz (**Figure 20**). The former is a standard parameter for the classification of ground-types in most building codes and in ground motion prediction equations. The latter is a parameter useful for the empirical estimation of the site-response and to assess the sensitivity of the seismic wave-field to the different depths. It has to be noticed that these two parameters are derived separately from all the best S-wave velocity models obtained from the inversion, and the results is finally averaged to improve statistics.

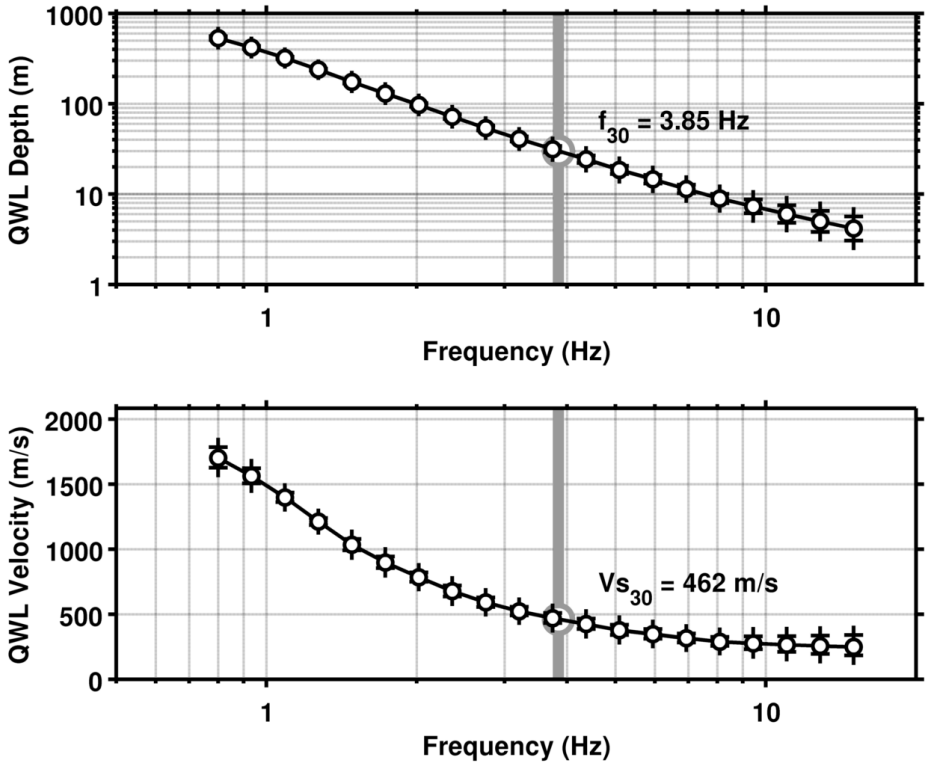

Figure 20 - *Quarter-wavelength representation of the inverted S-wave velocity profiles. On top the depth-frequency dependency. On bottom the QWL average velocity.*

12. Amplification models

Site amplification functions have been computed using two different approaches: the S-wave transfer function for vertical propagation and the quarter-wavelength amplification (Figure 21). In general the first method is used to evaluate the resonance characteristics of the site, while the second is more useful to assess the effect of the velocity contrasts between the lowermost rock layer (as reference) and the different QWL averaging depths. The results from the two methods are comparable, even if the transfer function provides a slightly larger amplification between 1 and 10Hz, because of the presence of some weak resonance in this frequency band. At high frequencies (the plateau regions) both methods provides a maximum average amplification of about 3. It has to be notice that the amplification functions do not include attenuation at this stage of the analysis, as the quality factors of the site are unknown.

Averaging depth	Vs-mean (m/s)	S.D.
5	271.96	46.21
10	299.67	18.05
15	350.92	23.40
20	391.02	19.77
25	430.45	21.15
30	**463.08**	**21.30**
40	518.25	17.19
50	573.15	20.12
75	692.52	19.21
100	795.89	18.62
150	961.33	24.26
200	1107.69	17.56

Table 1 - *Average travel time velocities at different depths. Vs30 is highlighted.*

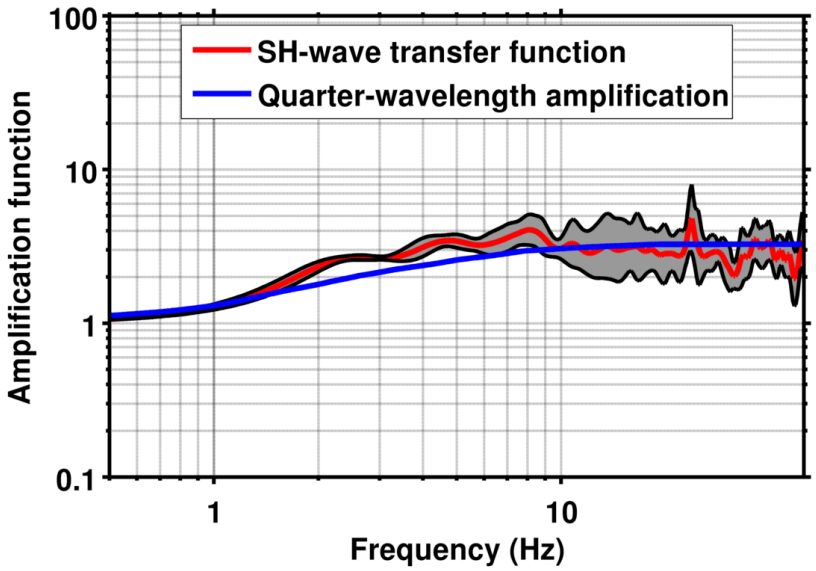

Figure 21 - *Comparison of amplification functions computed using the SH-wave transfer function and the quarter-wavelength formalism on the inverted velocity models. The functions are referenced to lowermost velocity layer.*

The SH-wave transfer function was then corrected for the Swiss rock reference velocity profile as defined in Poggi et al. (2011), according to the procedure described in Edwards et al. (2013). Given the lower velocities in the uppermost part of the Stiegenhof profile compared to the Swiss reference, the final corrected amplification function results in a general deamplification, with a maximum factor of about 0.6 at the plateau region (**Figure 22**).

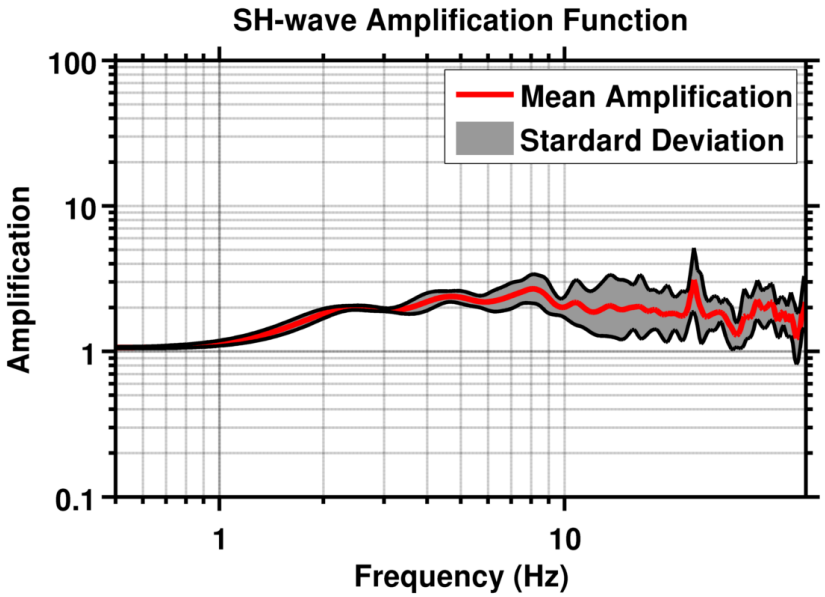

Figure 22 - *Correcting the SH-wave transfer function for the Swiss (rock) reference conditions (Poggi et al. 2011). The final corrected function shows a clear deamplification, with a maximum factor of about 0.6 at high frequencies.*

13. Comparing active and passive seismic results

The best model obtained from the inversion of surface waves from ambient vibration analysis has been finally compared with independent results from different active seismic techniques, including borehole VSP analysis, MASW, and refraction tomography (see attached report). At shallow depths, all the models from the different methods are consistent (**Figure 23**). Particularly, the VSP model shows the best match with the passive seismic result, with the exception of the first 10m, where VSP cannot resolve the details but only the average Vs velocity. Also MASW provided comparable models, but only down to a depth of about 25~30m, which has to be considered the maximum resolving depth of the method. This can be seen when comparing the dispersion curves obtained with ambient vibration array measurements and MASW, which overlap between 8Hz and 15Hz (**Figure 24**). Active MASW cannot excite surface waves at lower frequencies.

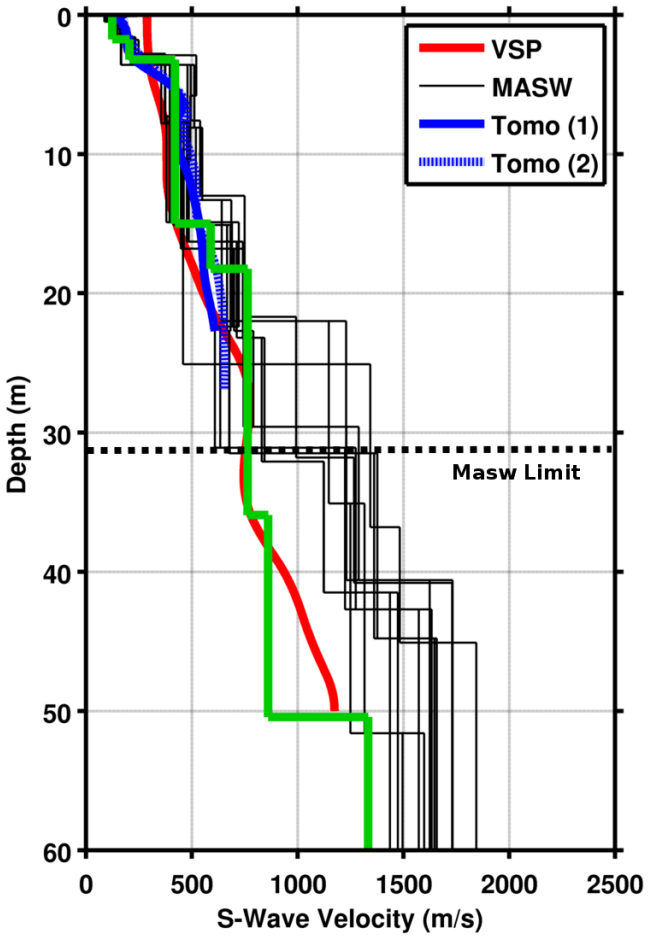

Figure 23 - *Comparison between the best fitting model (in green) from the inversion of passive surface waves with the results from different independent active seismic methods. The reliability region of the MASW method is explicitly presented, to account for the resolution limits of the method.*

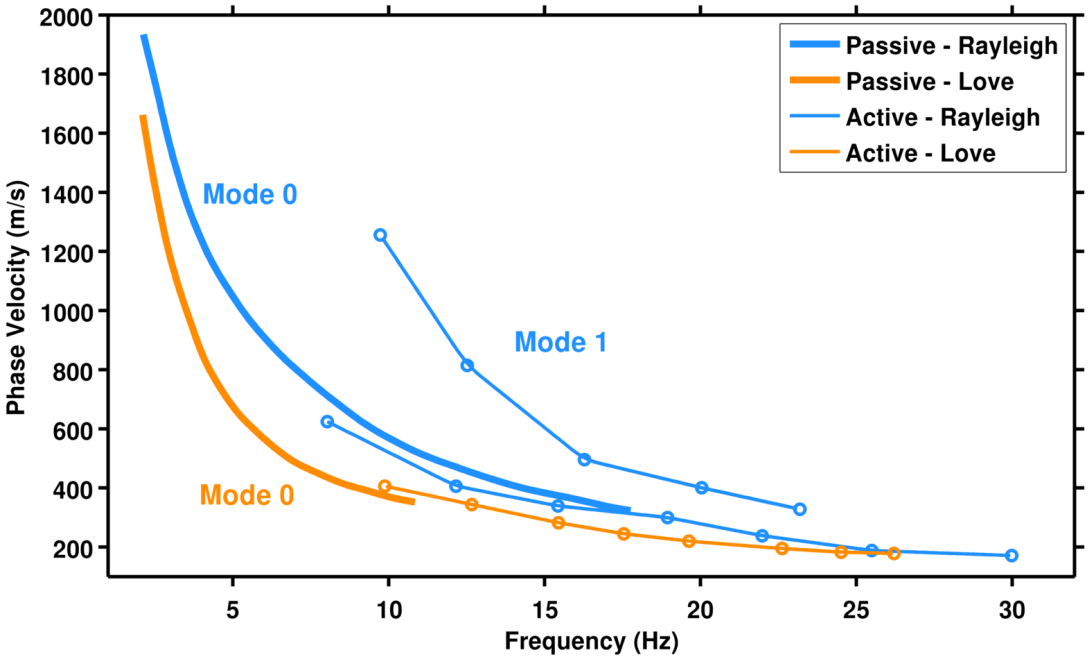

Figure 24 - *Comparison between the dispersion curves (Rayleigh and Love) from active and passive surface waves analysis. The lower resolution limit of MASW is roughly 8~10Hz in this case.*

REFERENCES

Capon, J., 1969. High resolution frequency wavenumber spectrum analysis, Proc. IEEE, 57, 1408-1418.

Burjanek, J., G. Stamm, V. Poggi, J.R. Moore, and D. Fäh [2010], "Ambient vibration analysis of an unstable mountain slope", Geophys. J. Int., Vol. 180, pp. 820-828.

Edwards, B., C. Michel, V. Poggi and D. Fäh (2013). Determination of Site Amplification from Regional Seismicity: Application to the Swiss National Seismic Networks. Accepted for publication in Seismological Research Letters.

Joyner, W. B., R. E. Warrick and T. E. Fumal (1981). The Effect of Quaternary Alluvium on Strong Ground Motion in the Coyote Lake, California, Earthquake of 1979, Bulletin of the Seismological Society of America, 71, 1333-1349.

Poggi, V., B. Edwards and D. Fäh (2011). Derivation of a Reference Shear-Wave Velocity Model from Empirical Site Amplification, Bulletin of the Seismological Society of America, 101, 258-274.

Poggi, V. and Fäh D., 2010. Estimating Rayleigh wave particle motion from three-component array analysis of ambient vibrations. Geophys. J. Int., 180-1, 251-267.

APPENDIX A

Borehole log

magma ag

Bohrung Stiegenhof STI-1, 8495 Oberembrach ZH
Geologisches Profil 1:500

Koordinaten:	691'578/261'495 (gemäss E-Mail Nagra, Herwig Müller, 11.10.2012)
Höhenlage:	Oberkante Terrain Bohrung ca. 635 m (aus LK 1:25'000 herausgelesen)
Bohrfirma:	Hastag St. Gallen
Bohrart:	~~Rotary-Spülbohrung, Spülmedium Luft, z.T. Wasser~~
Ausführung:	5./16.10.2012
Bohraufsicht:	Herwig R. Müller, Nagra
Probenentnahme:	Melissa Schwab, Nagra
Geologische Aufnahme:	17./18.10.2012, Thomas Gubler, magma AG, 8005 Zürich

Legende

- Feinsandstein
- silitiger Feinsandstein
- feinsandiger Siltstein, Siltstein (z.T. tonig)
- toniger Siltstein

US: Überschwemmungsablagerungen
RG: Rinnengürtel
DFR: Durchbruchsfächer
LAK: Seeablagerungen
H: Hörnli-Schüttung
E–W-Gls: E–W-Glimmersand-Schüttung